**Author(s):** Napari, Mari; Lahtinen, Manu; Veselov, Alexey; Julin, Jaakko; Østreng, Erik; Sajavaara, Timo

**Title:** Room-temperature plasma-enhanced atomic layer deposition of ZnO : Film growth dependence on the PEALD reactor configuration

**Year:** 2017

**Version:**

**Please cite the original version:**

Napari, M., Lahtinen, M., Veselov, A., Julin, J., Østreng, E., & Sajavaara, T. (2017). Room-temperature plasma-enhanced atomic layer deposition of ZnO : Film growth dependence on the PEALD reactor configuration. Surface and Coatings Technology, 326(Part A, October), 281-290. https://doi.org/10.1016/j.surfcoat.2017.07.056


# Room-temperature plasma-enhanced atomic layer deposition of ZnO: Film growth dependence on the PEALD reactor configuration

Mari Napari, Manu Lahtinen, Alexey Veselov, Jaakko Julin, Erik Østreng, Timo Sajavaara

PII: S0257-8972(17)30746-6
DOI: doi:10.1016/j.surfcoat.2017.07.056
Reference: SCT 22542

To appear in: *Surface & Coatings Technology*

Received date: 9 March 2017
Revised date: 9 June 2017
Accepted date: 23 July 2017

Please cite this article as: Mari Napari, Manu Lahtinen, Alexey Veselov, Jaakko Julin, Erik Østreng, Timo Sajavaara, Room-temperature plasma-enhanced atomic layer deposition of ZnO: Film growth dependence on the PEALD reactor configuration, *Surface & Coatings Technology* (2017), doi:10.1016/j.surfcoat.2017.07.056

# Room-temperature plasma-enhanced atomic layer deposition of ZnO: Film growth dependence on the PEALD reactor configuration

Mari Napari[a,*], Manu Lahtinen[b], Alexey Veselov[c], Jaakko Julin[a,1], Erik Østreng[c], Timo Sajavaara[a]

[a]*Department of Physics, University of Jyväskylä, PO Box 35, FI-40014 University of Jyväskylä, Finland*
[b]*Department of Chemistry, University of Jyväskylä, PO Box 35, FI-40014 University of Jyväskylä, Finland*
[c]*Picosun Oy, Masalantie 365, FI-02430 Masala, Finland*

**Abstract**

Room-temperature plasma-enhanced atomic layer deposition (PEALD) of ZnO was studied by depositing the films using diethylzinc and $O_2$ plasma from inductively-coupled plasma (ICP) and capacitively-coupled plasma (CCP) plasma source configurations. The CCP-PEALD was operated using both remote and direct plasma. It was observed that the films deposited by means of remote ICP and CCP were all highly oxygen rich, independently on plasma operation parameters, but impurity (H, C) contents could be reduced by increasing plasma pulse time and applied power. With the direct CCP-PEALD the film composition was closer to stoichiometric, and film crystallinity was enhanced. The ZnO film growth was observed to be similar on silicon, polycarbonate and poly(methyl methacrylate) substrates, but changes in polymer

*Corresponding author: Mari Napari, Department of Physics, P.O. Box 35, FI–40014, University of Jyväskylä, Finland. tel:+358 40 805 40 97, e-mail: mari.napari@jyu.fi

[1]Present address: Institute of Ion Beam Physics and Materials Research, Helmholtz-Zentrum Dresden-Rossendorf, PO Box 510119,01314 Dresden, Germany

surface morphology indicate plasma-induced damage during the deposition due to exposure to ion bombardment when direct plasma was applied.

*Keywords:* Plasma-enhanced atomic layer deposition, Zinc oxide, Inductively-coupled plasma, Capacitively-coupled plasma

## 1. Introduction

Low-temperature deposition processes are of special interest for applications where temperature-sensitive substrates, e.g. polymers and other organic materials are used. Atomic layer deposition is well suited for these applications, including organic photovoltaics and organic light emitting diodes, as it produces thin, conformal, and pinhole-free films [1]. Low-temperature ALD typically refers to temperatures $\leq 150$ °C, however, some applications benefit from coatings where no substrate heating is required, i. e. to reduce the film stress caused by thermal expansion of the substrate [2, 3]. Room-temperature thermal ALD processes have been established to some materials, mainly metal oxides such as $Al_2O_3$ [4, 5, 6], $SiO_2$ [7], and ZnO [8, 9], but these typically suffer from low film growth and require long processing times, especially when water is used as a reactant.

Plasma-enhanced ALD (PEALD) has been suggested as a solution to overcome these issues, and it has demonstrated to produce high quality films at room temperature [2], besides a variety of metal oxides e. g. $TiO_2$ [10], $HfO_2$ [11] and $WO_3$ [12], also of materials not achievable by thermal ALD e. g. Pt [13] and Ta [14]. PEALD relies on high reactivity of the plasma species, mainly the excited neutral atoms and molecules, referred to as plasma radicals. It has also been shown that the film growth is enhanced and properties improved when exposed to bombardment of plasma ions [15, 16]. Also energetic UV/VUV radiation is generated in the plasma, which can be beneficial to the film growth (i. e. photo-assisted ALD [17, 18, 19]) but can also, similarly to the ion bombardment, cause degradation of the substrate and the growing film [20, 21]. In commercial PEALD reactors plasma is typically gen-

erated by radio frequency (RF) inductively- or capacitively-coupled plasma sources (ICP and CCP, respectively), though microwave, electron cyclotron resonance (ECR), and hollow-cathode plasma sources are also used [22].

The initial plasma properties, e. g. plasma density and temperature, are strongly dependent on plasma source configuration. The density of the reactive species is also influenced by operation parameters, such as gas composition, driving frequency, pressure, and the reactor geometry [23]. In addition, the type of the PEALD setup, where the substrate is in contact with an active plasma (i. e. direct plasma) or with plasma "afterglow" (i. e. remote plasma) determines the film growth and properties [24]. The afterglow region can be defined as a volume where no power is applied and the local electron temperature is too low to cause ionization.

In this work the effect of the different reactor configurations on the growth and properties of room-temperature PEALD of ZnO films was studied. The films were deposited with remote plasma using ICP- and CCP-PEALD configurations, and with direct plasma CCP-PEALD. To investigate viability of the room-temperature PEALD of ZnO to temperature-sensitive materials, all the depositions were made on two common commercial polymers, polycarbonate and poly(methyl methacrylate), in addition to Si wafers. The possible plasma-induced damage was studied by investigating changes in surface morphology of the ZnO coated polymer surface.

## 2. Materials and Methods

### *2.1. Thin film deposition*

All the depositions were done on 1/4 of 150 mm Si(100) wafers, and commercial grade polycarbonate (PC, 2 mm Quinn Plastics) and poly(methyl methacrylate) (PMMA, 1 mm Evonik Plexiglas GT) substrates cut to 20 mm $\times$ 20 mm pieces. Prior to the deposition the polymer substrates were cleaned with isopropanol and dried with $N_2$ to remove possible residues of protective foils, and held in vacuum for removal of the absorbed water. Each deposition consisted of 600 PEALD cycles (except ICP-PEALD 3 and 6 s with 2000 W plasma power, where 1200 cycles were deposited) with diethylzinc (DEZ, $(C_2H_5)_2Zn$, $\geq$ 99 % Volatec and $\geq$ 95 % Strem Chemicals Inc. for ICP- and CCP-PEALD depositions, respectively) and $O_2$ plasma at room-temperature i. e. without substrate heating.

#### *2.1.1. ICP-PEALD*

The PEALD with inductively-coupled plasma was performed using Picosun™ R-200 Advanced. The plasma was generated with RF ICP plasma generator with maximum output power of 3 kW, using an automatic frequency matching (1.7–3.0 MHz). Distance between the plasma source and substrate was ca. 50 cm. For the depositions a flow of 140 sccm $O_2$ ($\geq$99.999 %) was fed to the plasma generator with Ar carrier gas (80 sccm). The reactor pressure was maintained at 5 mbar with continuous $N_2$ flow, which was also used for purging. The depositions were done with plasma powers of 500, 1000, and 2000 W with plasma pulse lengths of 6 and 11 s each, and additionally films with 3 s plasma pulses were deposited using powers of 500 and 2000 W. One

PEALD cycle consisted of 0.1 s DEZ pulse and subsequent 8 s purge followed by the plasma pulse and 10 s purge.

### *2.1.2. CCP-PEALD*

Beneq TFS-200 reactor, equipped with capacitively-coupled plasma unit with 13.56 MHz RF power source (CESAR 133, Advanced Energy) and impedance matching network (Navio, Advanced Energy) was used for CCP-PEALD depositions. The depositions were done both with direct plasma, where the substrates were placed on a grounded electrode at a distance of 35 mm from the powered electrode, and with the remote CCP setup, where a grid (aperture diameter 1.5 mm, spacing 2.0 mm, transparency ca. 50%) was positioned to separate the substrates from the plasma volume. The electrode–grid distance was set to 35 mm and the grid–substrate distance was 10 mm. The $O_2$ ($\geq$99.999 %) plasma gas (50 sccm) was fed to deposition chamber via electrode showerhead. The chamber pressure was maintained at 5 mbar with continuous $N_2$ flow, which was also used for purging. Plasma powers of 50, 100, and 200 W were used for depositions with pulse lengths of 1, 3, and 6 seconds each with the remote CCP-PEALD, and 3 and 6 s when the direct plasma was used. One PEALD cycle consisted of 0.5 s DEZ pulse, 15 s purge, followed by the plasma pulse and the subsequent purge. The purge length was adjusted to minimize the cumulative heating of the substrates during the plasma pulses, being 10–30 s, depending on the plasma power and pulse length. To compare the effect of the gas feed on the ZnO growth in the remote CCP-PEALD, a set of samples were deposited using $N_2$ flow of 50 sccm through the electrode showerhead while the $O_2$ was fed to the chamber via precursor inlet 0.5 s after the plasma ignition. The plasma pulse length was

3 s, with plasma powers of 50, 100, and 200 W. Other deposition parameters were as described above. In addition, degradation of polymers by the plasma was studied by exposing the substrates to the pulsed direct plasma with total exposure time of 15 min. The effect of plasma UV irradiation was investigated under the same conditions by protecting the substrates from plasma particles with 3 mm thick $MgF_2$ window (Eksma Optics).

### *2.2. Film characterization*

For growth per cycle determination ZnO films on Si substrates were measured with optical ellipsometer (Rudolph AutoEL III, laser wavelength 632.8 nm). The Zn areal densities of the films on different substrates were measured with Rutherford backscattering spectrometry (RBS) with 1.6 MeV $He^+$ incident ion beam. The ion fluence was normalized to beam chopper and Si substrate signal. The elemental composition of the films was measured using time-of-flight elastic recoil detection analysis (ToF-ERDA) [25] with 13.6 MeV $^{79}Br^{7+}$ ion beam, and the data were analyzed using Potku software [26], taking into account elemental losses during the measurement. Chemical composition of light element impurities was measured with attenuated total reflectance Fourier transform infrared spectroscopy (ATR-FTIR) (Bruker Alpha Platinum with diamond crystal as the internal reflectometer). Powder X-ray Diffraction (XRD) measurements were done using PanAlytical X'Pert PRO diffractometer with Cu K$\alpha_1$ (8.047 keV) incident X-ray. Surface topography of the samples was studied using atomic force microscopy (AFM, Bruker Dimension Icon).

## 3. Results

### *3.1. Film growth*

The GPC of the ZnO deposited using the remote ICP-PEALD, and the remote and direct CCP-PEALD are presented in Fig. 1.

The GPC of the ICP-PEALD ZnO changes as a function of the plasma power (Fig. 1(a)). The maximum GPC of 0.73 Å/cycle was achieved with 1000 W delivered power and 11 s plasma pulses. Increase in the power to 2000 W results in a drop in the GPC values down to 0.45–0.55 Å, depending on the plasma pulse length. The increase in the GPC when the plasma pulse length is increased can indicate an incomplete surface saturation during the $O_2$ plasma pulses. The GPC values of the films deposited with remote CCP-PEALD (Fig. 1(b)) using low plasma powers of 50 and 100 W are between 0.55–0.85 Å, being higher with longer plasma pulse lengths. At these plasma powers the gas feed distribution shows no ~~significant~~ effect on the film growth rates. Using 200 W plasma power with longer plasma pulses ($\geq$ 3 s) results in significant thickness variation in the deposited films and increases the average GPC, which was observed in the films deposited using the both gas feed distributions. The film thickness variations were observed as local non-uniformities, namely as 'spots' of thicker film located in the regions where the plasma gas was fed through the showerhead. Similar effect in the corresponding CCP-PEALD setup has also been reported e. g. by Bosund et al. [27]. The GPC values with direct CCP-PEALD are 1.15–1.35 Å already with 3 s pulses, and increase up to 1.45 Å when longer plasma pulses are applied. The GPC values are generally lower than reported in the literature for low-temperature PEALD ZnO (1.5–2.5 Å) deposited at

temperatures $\leq$ 100 °C [28, 29, 30, 31, 32], but comparable with studies of thermal ALD ZnO with deposition temperatures below 50 °C [8, 33, 34]. The detected low GPC is most probably due to the lower reactivity of the DEZ at low-temperatures [8, 35] and incomplete surface reactions during plasma pulses [36].

In low-temperature thermal ALD the growth of ZnO depends on substrate material. The initial nucleation of ZnO on polymer substrate has been reported to be delayed at low deposition temperatures [37], due to the lack of reactive sites on the polymer surface [38, 39]. To investigate if this significant delay applies also to the room-temperature PEALD of ZnO, the Zn content of the films was measured with Rutherford backscattering spectrometry (RBS) from the films deposited on Si, PMMA, and PC substrates.

Figure 2 shows the Zn areal density of the films on different substrates, expressed as Zn intake per cycle with units of $10^{15}$ atoms per cm$^2$. It can be seen that the Zn content corresponds to the GPC values independent on the substrate material. It has been demonstrated, that in low-temperature thermal ALD of ZnO from DEZ and water on PMMA the nucleation delay can be up to hundreds of cycles, followed by island-type growth [37]. Such differences in the Zn intakes cannot be observed in the PEALD ZnO films on PMMA and PC, which indicates that the growth is more similar on all studied substrates without significant delays in nucleation and initial film growth. The only notable differences in the Zn intake between the substrates are detected with direct CCP-PEALD with 50 and 100 W plasma power (Fig. 2(c)), and when ICP-PEALD with 2000 W power is used. In these cases the Zn content on the PMMA substrates is lower than on Si and PC.

*3.2. Composition analysis*

Dependence between the PEALD setup and ZnO film composition was studied by means of time-of-flight elastic recoil detection analysis (ToF-ERDA) and the results are collected in Tables I, II, and III.

The films deposited with ICP-PEALD, as seen in Table I, contain high amount of hydrogen and carbon impurities, but the concentrations are reduced when longer plasma pulses are applied. Small $< 1\%$ amounts of nitrogen and fluorine were also detected. The F content in the films is assumed to be of instrumental origin, most probably from O-ring gaskets. All ICP-PEALD films are oxygen rich with O/Zn ratios from 1.8 up to 2.8. The lowest O/Zn ratio was achieved with 2000 W plasma power, but it can be observed, that the increase in the plasma power and pulse length results in increase in not only the Zn content but in the amount of O as well.

The ToF-ERDA results of remote CCP-PEALD ZnO films are presented in Table II. These films are oxygen rich ZnO, similarly to ICP-PEALD films, but the O/Zn ratios are generally smaller and vary between 1.2 and 2.3. The impurity contents of H and C are comparable to ICP-PEALD deposited films, but N content appears slightly higher, being up to 5 % in the films deposited using 1 s plasma pulses, independently on the applied power. The gas feed distribution has no effect on the ZnO composition. Films with the lowest impurity contents and improved O/Zn ratios were deposited with direct CCP-PEALD (Table III). The films deposited with the 200 W power with 6 s pulses, both with the remote and direct CCP-PEALD setups, are alike in composition as well as in growth (Fig. 1(b) and (c)). This indicates that the thickness non-uniformity is due to the presence of a direct plasma

component on the deposition surface even when the remote CCP-PEALD setup with the grid was used.

The H and C impurities and high oxygen to metal ratios are typical for remote PEALD metal oxide films deposited with metal-organic precursors and $O_2$ plasma at room-temperature [2, 3]. The hydrogen content in the films has been explained by high density of surface OH groups created during the plasma exposure, that remain incorporated in the film, whereas the carbon impurities originate from the incomplete reactions of the metal precursor and from the re-deposition of by-products [2, 40, 41]. Besides by increasing the plasma pulse time, surface reaction enhancement and subsequent reduction of film impurities is also efficient when the direct plasma is applied, as presented in Table III.

To see if the plasma configuration affects the chemical composition of film impurities, the ZnO films were qualitatively studied by means of ATR-FTIR. To ensure a good signal to background ratio, the films deposited on the polymer substrates were measured, as the softer and more elastic substrate materials enabled a good contact between the film and the diamond crystal reflector. Spectra of untreated PMMA and PC sheets were used as references. Figure 3 shows selected FTIR absorption spectra of the films after substrate signal subtraction. The broad absorption appearing in all the spectra at 3600–3000 $cm^{-1}$ belongs to $-OH$ stretching, while the increase in absorbance at the range 1750–1300 $cm^{-1}$ is associated mainly to the CO containing species, with possible attribution of the $-CH_3$ C–H bending at 1400–1350 $cm^{-1}$ and 1470–1430 $cm^{-1}$. However, no increased absorbance arising from the $-CH_3$ groups is detected at 2950–2800 $cm^{-1}$ (streching) and

$\sim$1200 cm$^{-1}$ (deformation) [42], which indicates that the OH-groups are the main contributor to the measured hydrogen content in the films. As the DEZ precursor can infiltrate to the polymer sub-surface and react there with the functional groups of the polymer, the negative features in the difference spectra can be results of the consumption of these groups, e. g. C=O and C–O–R ester groups of PMMA [43].

Figures 3(a) and 3(b) show the ATR-FTIR spectra of the films deposited with ICP-PEALD using 500 W and 2000 W plasma power with 6 s pulses, respectively. At lower deposition plasma powers C=O absorption at $\sim$1660–1600 cm$^{-1}$ appears dominant together with the COO$^-$ at 1550 cm$^{-1}$ [3, 42], while the increase in the plasma power increases relative IR absorption of carbonate C–O stretching at 1500–1350 cm$^{-1}$ [44, 45]. It was observed that the increase in the plasma pulse length did not have an effect on the relative absorption intensities of different species. An example ATR-FTIR spectrum of the films deposited using remote CCP-PEALD is presented in Fig. 3(c). All the films deposited with the remote CCP-PEALD expressed strong OH contribution and presence of CO species, similarly to ICP-PEALD films. In the case of remote CCP-PEALD neither the applied plasma power nor the plasma pulse length were observed to affect the relative IR absorption peak intensities of different species. The presence of nitrogen in the CCP-PEALD films can be seen as a peak at 2200 cm$^{-1}$ attributed to nitrile C≡N bond [46], and the peak intensity was found to correlate with the ToF-ERDA measured N content. The absence of this feature in the spectra of the ICP-PEALD films with similar N content indicates the formation of NH or NO species, detected in N-doped ZnO [47], but these cannot, however, be distinguished

in the obtained spectra in small concentrations. The origin of the nitrogen containing compounds is assumed to be in the formation of reactive N species in the plasma, their density at the substrate being dependent on the used PEALD reactor configuration and the plasma gas mixture. A change in the gas feed distribution in remote CCP-PEALD, while not affecting the total carbon content in the films (Table II), results in a relative increase in the C = O contribution (Fig. 3(d)). The films grown with the direct CCP-PEALD show similar features as detected in the ICP-PEALD and remote CCP-PEALD films (Fig. 3(e)). A decrease in impurity content can be seen as a reduction in the total absorption intensity despite the increase in the film thicknesses. The high content of OH and carbonaceous species are reported to cause a decrease in the conductivity, and carrier concentration and mobility [36, 40], and can thus prevent the use of the room-temperature deposited films in electronic applications as such.

The results are in agreement with earlier reports of low-temperature PEALD of metal oxides with metal-organic precursors and $O_2$ plasma. In the studies of reaction mechanisms during PEALD of $Al_2O_3$ Heil et al. showed that the oxidation occurs via combustion-like reactions, where the plasma radicals react with the precursor ligands forming e. g. $H_2O$ and $CO_2$ as by-products [48]. Reported *in situ* infrared spectroscopy studies have shown that the surface OH groups, created during the $O_2$ plasma pulse act as reactive sites for the precursor adsorption together with the carbonate species that are formed as intermediates in the combustion-like reactions [42, 45]. The carbonate species can be decomposed upon prolonged plasma exposure, resulting in reduced impurity content in the films [49]. However, as the room-

temperature thermal ALD suffers from the inefficiency caused by the long purge times needed for the efficient water removal, also the increased plasma pulse times, up to minutes of exposure, compromise the processing efficiency. The long plasma pulses also increase the possibility of the substrate and film damage by the UV/VUV irradiation and ion bombardment.

### *3.3. Structural analysis*

The structure of the films was investigated using powder-XRD. Figure 4 presents the XRD patterns of the films deposited on Si substrates. The films deposited with ICP-PEALD appear mostly amorphous (Fig. 4(a)), with a slight indication of a polycrystalline structure, seen as a small peak originating from the (002) reflection in the film deposited with 2000 W plasma power. Similarly, as seen in Fig. 4(b) remote CCP-PEALD results in amorphous films, with exception of the film deposited using 6 s 200 W plasma pulses, that exhibits strongly the hexagonal wurtzite structure. Correspondingly the patterns of the direct CCP-PEALD films show strong $a$- and $c$-axis plane orientation, shown as intense (100) and (002) peaks in Fig. 4(c), together with the appearance of (110) peak at $56°(2\theta)$ (not shown). The peak shift towards smaller angles may indicate change in the residual stress of the films when the higher plasma power is applied [50, 51].

Though the observed hexagonal structure is characteristic for ALD and PEALD films, the orientation, being either (100), (002), or (101) dominated, is influenced by e. g. the choice of precursor, pulse and purge times, substrate material, deposition temperature, film thickness, and different plasma configurations and conditions [52]. Hence the comparison between different studies is complicated. However, here the amorphous/crystalline structure

shows a strong correlation with the detected growth and composition of the films deposited with different PEALD configurations.

In order to compare the detected structures to film morphology, the films were imaged using AFM. Figures 5, 6, and 7 show examples of the surface structures of the ZnO films deposited on Si substrates with (a) ICP-,(b) remote CCP-, and (c) direct CCP-PEALD, corresponding to the XRD patterns in Fig. 4(a)–(c). ZnO deposition with ICP-PEALD results smooth films with small grain size ($\leq$ 10 nm). The film roughness increases from ca. 0.3 to 1.2 nm when the applied plasma power is increased. The plasma pulse length was observed to have a less significant effect on the surface roughness than the applied plasma power. A more comprehensive collection of the AFM measured surface RMS roughnesses is presented in table IV.

The films deposited with remote CCP-PEALD with moderate plasma power of 50 and 100 W consist of larger grains (diameter 30–40 nm), leading to an increase in the surface roughness as seen in Fig. 6(a) and (b). Similar film structure was observed with shorter plasma pulse times, also when 200 W power was applied. However, the film deposited with 6 s pulses shows a change in the surface structure (Fig. 6(c)), with reduction in the surface roughness and grain size similar to the films deposited with direct CCP-PEALD. As seen in Fig. 7(a)-(c) the applied power had no effect on the film surface structure, consisting small slightly elongated grains with surface roughness of ca. 2.5 nm on average, being also virtually independent on the applied plasma pulse length.

To investigate the viability of the PEALD ZnO on polymer substrates, the surface structure of the films deposited on the PMMA and PC substrates

were also imaged with AFM. Figures 8 and 9 present the films on PMMA and PC substrates, respectively. In both figures the films are deposited with (b) ICP-PEALD using 1000 W plasma with 11 s pulses, (c) remote CCP-PEALD, and (d) direct CCP-PEALD, both using 100 W plasma and 6 s pulses. Figures 8(a) and 9(a) show the surfaces of the uncoated PMMA and PC, respectively.

The used commercial grade PMMA has initially high surface roughness ($R_{RMS}$ =5–7 nm), featuring smaller (diameter 50–80 nm) round and larger (250–300 nm) 'donut-shaped' surface granulates. The films deposited with remote plasma, both with ICP- and CCP-PEALD show growth similar than detected with Si substrates (corresponding depositions in Figs. 5(b) and 6(b)). The grain-like growth is slightly emphasized, especially around the initial surface features of the PMMA, but no significant changes indicating a substrate damage during the plasma processing were detected. However, when the direct CCP-PEALD is applied, the surface roughness increases to $R_{RMS}$ ≈10 nm, as seen in Fig. 8(d), which indicates PMMA degradation under the ion bombardment during the deposition. This effect is less pronounced in the PC substrates, with initial roughness of ca. 0.4 nm, shown in Fig. 9, where the surface roughnesses after film deposition are comparable to the films deposited on Si substrates, also with direct CCP-PEALD. Thus the severeness of the surface damage can be considered to be dependent on the resilience of the polymer material to the plasma irradiation and ion bombardment.

No significant changes were observed with remote PEALD, which indicates that the surface damage is mainly attributed to the ion bombardment.

Moreover, also UV-radiation is created in the plasma, which can cause photodegradation of the polymer surfaces [53]. The effect of UV irradiation and the ion bombardment to the polymer surface was characterized by exposing the PC substrates to the direct CCP without film deposition. To isolate the effect of the UV, $MgF_2$ window was used to protect samples from plasma particles. The AFM images of the PC surfaces exposed to the UV irradiation and direct plasma are shown in Fig. 10. The surface roughness of the PC exposed to the UV through the $MgF_2$ window (Fig. 10(a)) was measured to be $\sim$0.45 nm, being similar to the untreated reference (Fig. 9(a)). The sample exposed to the direct plasma, however, shows a change in the surface morphology (Fig. 10(b)), with an increase in RMS roughness to ca. 1.3 nm. In comparison, the RMS surface roughness of PMMA increased to $\sim$35 nm after the similar direct plasma exposure (not shown), which emphasizes the sensitivity of PMMA to the ion bombardment.

The exposure tests thus support the hypothesis of the ion bombardment being the main contributor to the plasma-induced damage. The exposure to the plasma was observed to cause damage to PC, even when no changes were observed in the samples with PEALD ZnO films. However, during the ZnO deposition the film itself will protect the substrate from further plasma damage after a certain thickness [54]. Also the possibility of the UV-induced damage, i. e. photochemical changes in the polymers, cannot be excluded solely by studying the surface morphology of the samples.

## 4. Discussion

In room-temperature PEALD, where no additional thermal energy is provided to enhance the reactivity, the effect of the plasma on the film growth and properties is substantial. The observed differences in the films underline the role of energetic ions in the room-temperature PEALD. As presented, the growth and characteristics of the deposited ZnO films depend on the used PEALD setup. In the remote PEALD, both with ICP- and CCP-configurations the film growth and properties were alike. The low growth rate, high content of residual H and C in oxygen rich films, and the amorphous structure can be considered as consequences of the inadequate energy deposition for the surface reactions during the plasma pulses.

In the remote ICP-PEALD used in this study the high operation pressure (5 mbar) results in that despite the high plasma density the ion flux and energy deposition to the substrate can be considered negligible. Hence, the film growth is governed mainly by the neutral oxygen species, that can be either ground state oxygen atoms or even $O_2$ molecules [56] or exited species i. e. plasma radicals, mainly the low energy metastable O and $O_2$ [55]. The density of these species is restricted by the de-excitation processes in the plasma and afterglow volume as well as the recombination reactions at the surfaces [57].

The assumption of low-energy metastable governed growth gets support when considering the films deposited using the remote and direct CCP-PEALD, under the same pressure of 5 mbar. In the used remote setup the substrate is placed in a distance of 1 cm from the grid that confines the plasma volume. The grid allows the ions to pass through the holes and the

flux is restricted by the grid transparency. The energy of the ions is mainly lost in the collisions and in the ion recombination within the volume below the grid. However, it is plausible that a small fraction of the ions can contribute to the surface reactions, but by comparing the films deposited with the remote and direct CCP-PEALD setups, the effect of this fraction to the film growth is not substantial. The small distance between the plasma volume and the substrate can also allow a flux of higher energy plasma radicals to the substrate.

The effect of the distance $x$ between the active (ionizing) plasma and the substrate to the number of specific species at the substrate ($N_s$) can be approximated as:

$$N_s = N_0 e^{-(\Sigma n_j \sigma_j)x}, \tag{1}$$

where $N_0$ is the initial number of the species created in the plasma, which is proportional to the plasma density $n_e$, and the production process rate coefficient $\langle \sigma v \rangle$. The amount of species consumed by processes such as de-excitation is described with the exponential function consisting of the density of the colliding species $n_j$ and the cross sections $\sigma_j$ of the processes. In this case, where the electron temperatures in the plasma are similar in both the CCP and ICP (1–5 eV), the $N_0$ is only dependent on the plasma density, being $10^9 - 10^{10}$ cm$^{-3}$ for the CCP and $10^{10} - 10^{12}$ cm$^{-3}$ for the ICP. As the majority of the species interactions occur with the neutral molecules, $n_{j,\mathrm{ICP}} = n_{j,\mathrm{CCP}}$ at the same pressure. Due to the exponential nature of the species consumption, the distance $x$ becomes the dominant factor. Thus, in this case the 50 cm distance from the ICP source results in the lower fluence

of ~~energetic~~reactive species to the substrate despite the higher initial plasma density. This, together with the plausible ion contribution, causes the small improvement in the film composition and differences in the film structure in the remote CCP-PEALD deposited films.

The anomalies in the film growth with remote CCP-PEALD with 200 W plasma power can be explained by a presence of a 'parasitic' active plasma component between the grid and the substrate. The generation of this plasma component is a result of the mode transition effect in the RF capacitive discharge [58, 59], and its effect on PEALD is reported in detail in Ref. [60]. The mode transition phenomena are not restricted to the CCP discharges, and the presence of characteristic E–H transition in the RF ICP was observed also in the system used for the ICP-PEALD (see Appendix). Though no significant changes were observed in the ZnO films deposited under different ICP modes, the reduction in the GPC and slightly enhanced crystalline structure between 1000 W and 2000 W applied powers may be results of changes in plasma parameters caused by the detected plasma mode transition, and the subsequent difference in the density/energy of the neutral species accounted for the film growth. However, the exact reason for the differences in the ZnO growth and properties between the two plasma modes remains yet unknown and will be a subject of future investigations.

## 5. Conclusions

ZnO films deposited by means of remote ICP- and CCP-PEALD were amorphous and had high O/Zn ratio from 1.6 up to 2.8 accompanied by high H and C impurity content, but the film composition was to some extent

improved with increased plasma pulse length and power. The film growth was similar on Si, PMMA, and PC substrates, indicating that the plasma activates the ZnO growth on polymers via increase in the reactive surface sites. This avoids the nucleation delay observed in low-temperature thermal ALD on polymers. Crystalline films were achieved with direct CCP-PEALD, but the exposure to ion bombardment caused roughening of the polymer surface. Therefore the room-temperature PEALD on sensitive substrates must compromise between the film quality and substrate damage. The slow film growth with remote PEALD can be connected both to the low reactivity of the diethylzinc precursor as well as to the insufficient energy deposition of the plasma species to the substrate. This is a result of the high pressure of the PEALD reactors that leads to an increase in the de-excitation processes consuming the energetic plasma radicals.

**Acknowledgements**

This work was supported by Academy of Finland Center of Excellence in Nuclear and Accelerator Based Physics (ref. num. 251353). V.-M. Hiltunen is acknowledged for Si reference AFM measurement.

## Appendix A. E–H transition in ICP-PEALD $O_2$(–Ar) plasma

In the electrostatic E mode, typically observed with low powers, the electric field is generated between the coil segments, making the plasma coupling capacitive. With increasing power over specific critical value the discharge transits into the electromagnetic H mode, where the coupling is inductive [61]. The mode transition to the capacitive E mode to the inductive H mode

increases the electron density in the plasma, and decreases the electron energy and plasma potential [62]. Subsequently to the deposition experiments the ICP mode transition in the $O_2$ plasma was investigated by optical emission spectroscopy (OES) in the visible wavelength range. The spectra were recorded with OceanOptics USB2000+ spectrometer, and the optical fiber was coupled to view the plasma perpendicularly at a distance of 5 cm below the plasma source. Figure 11 shows the recorded spectra with plasma powers of 500, 1000, and 2000 W. It was observed that at low powers (up to 1000 W) the optical emission spectra is dominated by Ar carrier gas, with the most intense line observed at 751 nm. When 2000 W power is applied the total optical intensity decreases and atomic oxygen at 777 nm becomes the dominant emission line.

Figure 12 shows the RF characteristics of the plasma generator (frequency, DC voltage, and DC current) as a function of the applied power, and the normalized peak intensities of Ar 751 nm and 811 nm lines, and O 777 nm line of the corresponding optical emission spectra. It can be seen that below 1000 W the output voltage remains constant while the current increases with applied power, indicating that the plasma is operated in the capacitive (E) mode. From 1250 W onwards the plasma is in the inductive (H) mode, and the plasma power increase is applied by increasing the DC voltage. The transition is accompanied by a drastic drop of Ar line intensities in the obtained OES spectra.

The selected intense Ar emission lines correspond to the decays of Ar excited to high energy levels. These energy levels can be occupied either by direct electron impact excitation or by ionization followed by recombi-

nation [63]. However, for these processes the threshold energies are above 13 eV [64], which means that in the capacitive E mode the contribution of the high-energy tail of the electron energy distribution is significant. After the transition to the H mode the intensities of these lines reduce drastically, indicating a reduction in the effective electron temperature, being in agreement with the reported changes in plasma parameters during the E–H mode transition. The increase in the O 777 nm line intensity corresponds to the increase in the (low-energy) electron dens ity as a function of the applied power.

## References

[1] K. L. Jarvis, P. J. Evans, Growth of thin barrier films on flexible polymer substrates by atomic layer deposition, Thin Solid Films 624 (2017) 111

[2] S. E. Potts, H. B. Profijt, R. Roelofs, W. M. Kessels, Room-temperature ALD of metal oxide thin films by energy-enhanced ALD Chem. Vap. Deposition 19 (2013) 1

[3] T. O. Kääriäinen, D. C. Cameron, Plasma-assisted atomic layer deposition of $Al_2O_3$ at room-temperature, Plasma Process. Polym. 6 (2009) S237

[4] M. Kot, C. Das, Z. Wang, K. Henkel, Z. Rouissi, K. Wojciechowski, H. J. Snaith, D. Schmeisser, Room-temperature atomic layer deposition of $Al_2O_3$: Impact on efficiency, stability and surface properties in perovskite solar cells, ChemSusChem 9 (2016) 3401

[5] X. Tang, L. A. Francis, Room-temperature atomic layer deposition of $Al_2O_3$ and replication of butterfly wings for photovoltaic application J. Vac. Sci. Technol. A 30 (2011) 01A146

[6] M. D. Groner, F. H. Fabreguette, J. W. Elam, S. M. George, Low-temperature $Al_2O_3$ atomic layer deposition, Chem. Mater. 16 (2004) 639

[7] J. W. Klaus, S. M. George, Atomic layer deposition of $SiO_2$ at room temperature using $NH_3$-catalyzed sequential surface reactions, Surface Science 447 (2000) 81

[8] J. Malm, E. Sahramo, J. Perälä, T. Sajavaara, M. Karppinen, Low-temperature atomic layer deposition of ZnO thin films: Control of crystallinity and orientation, Thin Solid Films 519 (2011) 5319

[9] T. Nam, J.-M. Kim, M.-K. Kim, H. Kim, Low-temperature atomic layer deposition of $TiO_2$, $Al_2O_3$, and ZnO thin films, J. Korean Phys. Soc. 59 (2011) 452

[10] K. Kikuchi, M. Miura, K. Kanomata, B. Ahmmad, S. Kubota, F. Hirose, Room-temperature atomic layer deposition of $TiO_2$ on gold nanoparticles, J. Vac. Sci. Technol. A 35 (2017) 01B121

[11] K. Kanomata, H. Ohba, P. P. Pansila, B. Ahmmad, K. Hiraha, F. Hirose, Infrared study of room-temperature atomic layer deposition of $HfO_2$ using tetrakis(ethylmethylamino)hafnium and remote plasma-excited oxidizing agents, J. Vac. Sci. Technol. 33 (2014) 01A133

[12] A. Strobel, H. D. Schnabel, U. Reinhold, S. Rauer, A. Neidhardt, Room-temperature plasma enhanced atomic layer deposition for $TiO_2$ and $WO_3$ films, J. Vac. Sci. Techol. A 34 (2016) 01A118

[13] A. J. M. Mackus, D. Garcia-Alonso, H. C. M. Knoops, A. A. Bol, W. M. M. Kessels, Room-temperature atomic layer deposition of platinum, Chem. Mater 25 (2013) 1769

[14] S. M. Rossnagel, A. Sherman, F. Turner, Plasma-enhanced atomic layer deposition of Ta and Ti for interconnected diffusion barreries, J. Vac. Sci. Technol. B 18 (2000)

[15] H. B. Profijt, W. M. M. Kessels, Ion bombardment during plasma-assisted atomic layer deposition, ECS Trans. 50 (2013) 23

[16] H. Kim, S. Woo, J. Lee, Y. Kim, H. Lee, I. J. Choi, Y.D. Kim, C. W. Chung, H. Jeon, Effect of DC bias on the plasma properties in remote plasma atomic layer deposition and its application to $HfO_2$ thin films, J. Electrochem. Soc. 158 (2011) H21

[17] J. C. Kwak, Y.-H. Lee, B.-H. Choi, Preparation of tantalum oxide thin films by photo-assisted atomic layer deposition, Appl. Surf. Sci. 230 (2004) 249

[18] B. H. Lee, S. Cho. J. K. Hwang, S. H. Kim, M. M. Sung, UV-enhanced atomic layer deposition of $ZrO_2$ thin films at room temperature, Thin Solid Films 518 (2010) 6432

[19] K. H. Yoon, H. Kim, Y.-E. K. Lee, N. K. Shrestha, M. M. Sung, UV-enhanced atomic layer deposition of $Al_2O_3$ thin films at low temperature for gas-diffusion barriers, RSC Adv. 7 (2017) 5601

[20] H. Ren, Y. Nishi, J. L. Shohet, Changes and defects in dielectric from ion and photon fluences during plasma exposure, Electrochem. Solid-State Lett. 14 (2011) H107

[21] H. B. Profijt, P. Kudlacek, M. C. M. van de Sanden, W. M. M. Kessels, Ion and photon surface interaction during remote plasma ALD of metal oxides, J. Electrochem Soc. 158 (2011) G88

[22] H. B. Profijt, S. E. Potts, M. C. M. Sanden, W. M. M. Kessels, Plasma-assisted atomic layer deposition: basics, opportunities, and challenges, J. Vac. Sci. Technol. A 29 (2011) 050801

[23] M. A. Liebermann, A. J. Lichtenberg, Principles of plasma discharges and materials processing, 2nd edition, Wiley, New York

[24] J. Kim, S. Kim, H. Kang, J. Choi, H. Jeon, M. Cho, K. Chung, S. Back, K, Yoo, C. Bae, Composition, structure, and electrical characteristics of $HfO_2$ gate dielectrics frown using the remote- and direct-plasma atomic layer deposition methods, J. Appl. Phys. 98 (2005) 094504

[25] M. Laitinen, M. Rossi, J. Julin, T. Sajavaara, Time-of-flight Energy spectrometer for elemental depth profiling Jyväskylä design, Nucl. Instrum. Meth. B 337 (2014) 55

[26] K. Arstila et al., Potku–New analysis software for heavy ion elastic recoil detection analysis, Nucl. Instrum. Meth. B 331 (2014) 34

[27] M. Bosund, T. Sajavaara, M. Laitinen, T. Huhtio, M. Putkonen, V.-M. Airaksinen, H. Lipsanen, Properties of AlN grown by plasma enhanced atomic layer deposition, Appl. Surf. Sci. 257 (2011) 7827

[28] J. Zhang, H. Yang, Q.-l. Zhang, S. Dong, J. K. Luo, Bipolar resistive switching characteristics of low-temperature grown ZnO thin films by plasma-enhanced atomic layer deposition, Appl. Phys. Lett. 102 (2013) 012113

[29] D. Kim, H. Kang, J.-M. Kim, H. Kim, The properties of plasma-enhanced atomic layer deposition (ALD) ZnO thin films and comparison with thermal ALD, Appl. Surf. Sci. 257 (2011) 3776

[30] M.-j. Jin, J. Jo, G. P. Neupane, J. Kim, K.-S. An, J. W. Yoo, Tuning of undoped ZnO thin film via plasma-enhanced atomic layer deposition and its application for an inverted polymer solar cell, AIP Advances 3 (2013) 102114

[31] P. C. Rowlette, C. G. Allen, O. B. Bromley, A. E. Dubetz, C. A. Wolden, Plasma-enhanced atomic layer deposition of semiconductor grade ZnO using dimethyl zinc, Chem. Vap. Deposition 15 (2009) 15

[32] S.-H. K. Park, C.-S. Hwang, H.-S. Kwack, J.-H. Lee, H. Y. Chu, Characteristics of ZnO thin films by means of plasma-enhanced atomic layer deposition, Electrochem. Solid State Lett. 9 (2006) G299

[33] T.-Y. Chiang. C.-L. Dai, D.-M. Lian, Influence of growth temperature on the optical and structural properties of ultrathin ZnO films, J. Alloys Compounds 509 (2011) 5623

[34] N. Y. Yuan, S. Y. Wang, C. B. Tan, X. Q. Wang, G. G. Chen, J. N. Ding, The influence of deposition temperature on growth mode, optical and mechanical properties of ZnO films prepared by the ALD method, J. Cryst. Growth 366 (2013) 43

[35] M. Vähä-Nissi, M. Pitkänen, E. Salo, E. Kenttä, A. Tanskanen, T. Sajavaara, M. Putkonen, J. Sievänen, A. Sneck, M. Rättö, M. Karppinen, A. Harlin, Antibacterial and barrier properties of oriented polymer films

with ZnO thin films applied with atomic layer deposition at low temperatures, Thin Solid Films 562 (2014) 331

[36] M. A. Thomas, J. B. Cui, Highly tunable electrical properties in undoped ZnO grown by plasma enhanced thermal atomic layer deposition, ACS Appl. Mater. Interfaces 4 (2012) 3122

[37] M. Napari, J. Malm, R. Lehto, J. Julin, K. Arstila, M. Lahtinen, T. Sajavaara, Nucleation and growth of ZnO by low-temperature atomic layer deposition J. Vac. Sci. Technol. A 33 (2015) 01A128

[38] A. K. Roy, D. Deduytche, C. Detavernier,Wetting transitions of polymers via thermal and plasma enhanced atomic layer depositions, J. Vac. Sci. Technol. A 31 (2013) 01A147

[39] H. C. Guo, E. Ye, Z. Li, M.-Y. Han, X. J. Loh, Recent progress of atomic layer deposition on polymeric materials, Mater. Sci. Eng. C Mater. Biol. Appl. 70 (2017) 1182

[40] S. M. Sultan, O. D. Clark, T. B. Masaud, Q. Fang, R. Gunn, M. M. A. Hakim, K. Sun, P. Ashburn, H. M. H. Chong, Remote plasma enhanced atomic layer deposition of ZnO for thin film electronic applications, Microelectronic Engineering 97 (2012) 162

[41] H. C. M. Knoops, K. de Peuter, W. M. M. Kessels, Redeposition in plasma-assisted atomic layer deposition: Silicon nitride film quality ruled by the gas residence time, Appl. Phys. Lett. 107 (2015) 014102

[42] E. Langereis, J. Keijmel, M. C. M. van de Sanden, W. M. M. Kessels,

Surface chemistry of plasma-assisted atomic layer deposition of $Al_2O_3$ studied by infrared spectroscopy, Appl. Phys. Lett. 92 (2008) 231904

[43] M. Biswas, J. A. Libera, S. B. Darling, J. W. Elam, New insight into the mechanism of sequential infiltration synthesis from infrared spectroscopy, Chem. Mater. 26 (2014) 6135

[44] V. R. Rai, S. Agarval, Surface reaction mechanisms during plasma-assisted atomic layer deposition of titanium dioxide, J. Phys. Chem. C 113 (2009) 12963

[45] V. K. Rai, V. Vandalon, S. Agarval, Surface reaction mechanisms during oxone and oxygen plasma assisted atomic layer deposition of aluminum oxide, Langmuir 26 (2010) 13732

[46] T. J. Coutts, X. Li, T. M. Barnes, B. M. Keyes, C. L. Perkins, S. E. Asher, S. B. Zhang, S.-U. Wei, S. Limpijumnong, Synthesis and characterization of nitrogen doped ZnO films grown by MOCVD, Ch 3 in Zinc oxide bulk, thin films and nanostructures, Ed. C. Jagadish, S. Pearton, 1st edition Elsevier, Oxford, 2006

[47] C. Lee, J. Lim, Dependence of the electrical properties of the ZnO thin films grown by atomic layer epitaxy on the reactant feed sequence, J. Vac. Sci. Technol. A 24 (2006) 1031

[48] S. B. S. Heil, P. Kudlacek, E. Langereis, R. Engeln, M. C. M. van de Sanden, W. M. M. Kessels, Appl. Phys. Lett. 89 (2006) 131505

[49] V. K. Rai, V. Vandalon, S. Agarval, Influence of surface temperature on

the mechanism of atomic layer deposition of aluminum oxide using an oxygen plasma and ozone, Langmuir 28 (2012) 350

[50] N. Samal, H. Du. R. Luberoff, K. Chetry, R. Bubber, A. Hayes, A. Devasahayam, Low-temperature ($\leq$ 200°C) plasma enhanced atomic layer deposition of dense titanium nitride films, J. Vac. Sci. Technol. A 31 (2013) 01A137

[51] S.-B. Zhu, Y. Geng, H.-L. Lu, Y. Zhangm Q.-Q. Sun, S.-J. Ding, D. W. Zhang, Effects of rapid thermal annealing on Hf-doped ZnO films grown by atomic layer deposition, J. Alloys Compounds 577 (2013) 340

[52] V. Miikkulainen, M. Leskelä, M. Ritala, R. L. Puurunen, Crystallinity of inorganic films grown by atomic layer deposition: Overview and general trends, J. Appl. Phys. 113 (2013) 021301

[53] C. Fozza, J. E. Klemberg-Sapieha, M. R. Wertmeier, Vacuum ultraviolet irradiation of polymers, Plasmas Polym. 4 (1999) 186

[54] T. O. Kääriäinen, D. C. Cameron, M. Tanttari, Adhesion of Ti and TiC coatings on PMMA subject to plasma treatment: Effect of intermediate layers of $Al_2O_3$ and $TiO_2$ deposited by atomic layer deposition, Plasma Process. Polym. 6 (2009) 631

[55] J. T. Gudmundsson, M. A. Liebermann, On the role of metastables in capacitively coupled oxygen discharges, Plasma Sources Sci. Technol. 24 (2014) 035016

[56] E. Janocha, C. Pettenkofer, ALD of ZnO using diethylzinc as metal-precursor and oxygen as oxidizing agent, Appl. Surf. Sci. 257 (2011) 10031

[57] M. J. Sowa, Role of plasma enhanced atomic layer deposition reactor wall conditions on radical and ion substrate fluxes, J. Vac. Sci. Technol. A 32 (2014) 01A106

[58] V. A. Lisovskiy, V. D. Yegorenkov, Alpha–gamma transition in RF capacitive discharge in low-pressure oxygen, Vacuum 74 (2004) 19

[59] X. Yang, M. Moravej, G. R. Nowling, S. E. Babayan, J. Panelon, J. P. Chang, R. F. Hicks, Comparison of an atmospheric pressure, radio-frequency duscharge operating in the $\alpha$ and $\gamma$ modes, Plasma Sources Sci. Technol. 14 (2005) 314

[60] M. Napari, O. Tarvainen, S. Kinnunen, K. Arstila, J. Julin, Ø. S. Fjellvåg, K. Weibye, O. Nilsen, T. Sajavaara, The $\alpha$ and $\gamma$ plasma modes in plasma-enhanced atomic layer deposition with $N_2$–$O_2$ capacitive discharges, J. Phys. D: Appl. Phys. 50 (2017) 095201

[61] J. Hopwood, Review of inductively coupled plasmas for plasma processing, Plasma Sources Sci. Technol. 1 (1992) 109

[62] Th. Wegner, C. Küllig, J. Meichsner, E–H transition in Argon/Oxygen inductively coupled RF plasmas, Contrib. Plasma Phys. 55 (2015) 728

[63] Z. M. Jelenak, Z. B. Velikić, J. V. Božin, Z. Lj. Petrović, B. M. Jelenković, Electronic excitation of the 750- and 811-nm lines of argon, Phys. Rev. E 47 (1993) 3566

[64] P. Palmeri, e. Biémont, Energy levels of high-/ states in neutral and singly ionized argon, Physica Scripta 51 (1995) 76

Table I: Elemental compositions of the remote ICP-PEALD ZnO films, measured using ToF-ERDA.

| P (W) | t (s) | H (at. -%) | C (at. -%) | N (at. -%) | F (at. -%) | O (at. -%) | Zn (at. -%) | O/Zn ratio |
|---|---|---|---|---|---|---|---|---|
| 500 | 3 | 26 ± 2 | 10 ± 1 | 0.4 ± 0.1 | 0.2 ± 0.05 | 46 ± 2 | 17 ± 1 | 2.8 ± 0.3 |
| 500 | 6 | 17 ± 1 | 10 ± 1 | 0.7 ± 0.1 | 0.1 ± 0.05 | 50 ± 2 | 22 ± 2 | 2.3 ± 0.3 |
| 500 | 11 | 16 ± 1 | 9 ± 0.5 | 0.7 ± 0.1 | – | 51 ± 2 | 22 ± 2 | 2.3 ± 0.4 |
| 1000 | 6 | 17 ± 1 | 10 ± 1 | 0.5 ± 0.1 | 0.1 ± 0.05 | 50 ± 2 | 22 ± 2 | 2.3 ± 0.2 |
| 1000 | 11 | 16 ± 1 | 8 ± 0.5 | 0.3 ± 0.05 | 0.1 ± 0.05 | 51 ± 2 | 24 ± 2 | 2.1 ± 0.2 |
| 2000 | 3 | 26 ± 2 | 9 ± 0.5 | 0.2 ± 0.05 | 0.6 ± 0.1 | 44 ± 2 | 20 ± 2 | 2.2 ± 0.3 |
| 2000 | 6 | 16 ± 1 | 8 ± 0.5 | 0.3 ± 0.05 | 0.6 ± 0.1 | 50 ± 2 | 25 ± 2 | 1.8 ± 0.2 |
| 2000 | 11 | 13 ± 1 | 6 ± 0.5 | 0.2 ± 0.05 | – | 53 ± 2 | 27 ± 2 | 2.0 ± 0.2 |

Table II: Elemental compositions of the remote CCP-PEALD ZnO films, measured using ToF-ERDA. The films denoted with (*) are deposited using the alternative $O_2$ feed distribution and plasma ignition using $N_2$.

| P (W) | t (s) | H (at. -%) | C (at. -%) | N (at. -%) | O (at. -%) | Zn (at. -%) | O/Zn ratio |
|---|---|---|---|---|---|---|---|
| 50 | 1 | 22 ± 1 | 12 ± 1 | 5 ± 0.5 | 43 ± 2 | 19 ± 1 | 2.3 ± 0.2 |
| 50 | 3 | 17 ± 1 | 6 ± 0.5 | 1 ± 0.2 | 48 ± 2 | 28 ± 2 | 1.7 ± 0.2 |
| 50* | 3 | 18 ± 1 | 8 ± 0.5 | 1 ± 0.2 | 48 ± 2 | 25 ± 2 | 1.9 ± 0.2 |
| 50 | 6 | 15 ± 1 | 6 ± 0.5 | 1 ± 0.2 | 48 ± 2 | 29 ± 2 | 1.7 ± 0.2 |
| 100 | 1 | 19 ± 1 | 11 ± 1 | 5 ± 0.5 | 43 ± 2 | 22 ± 2 | 2.0 ± 0.3 |
| 100 | 3 | 19 ± 1 | 6 ± 0.5 | 2 ± 0.2 | 47 ± 2 | 28 ± 2 | 1.7 ± 0.2 |
| 100* | 3 | 18 ± 1 | 7 ± 0.5 | 1 ± 0.2 | 48 ± 2 | 26 ± 2 | 1.9 ± 0.2 |
| 100 | 6 | 15 ± 1 | 6 ± 0.5 | 2 ± 0.2 | 48 ± 2 | 30 ± 2 | 1.6 ± 0.2 |
| 200 | 1 | 14 ± 1 | 8 ± 0.5 | 5 ± 0.5 | 46 ± 2 | 28 ± 2 | 1.7 ± 0.1 |
| 200 | 3 | 17 ± 1 | 8 ± 0.5 | 3 ± 0.2 | 46 ± 2 | 27 ± 2 | 1.8 ± 0.2 |
| 200* | 3 | 13 ± 1 | 5 ± 0.5 | 1 ± 0.2 | 48 ± 2 | 32 ± 2 | 1.5 ± 0.2 |
| 200 | 6 | 6 ± 0.5 | 2 ± 0.2 | 1 ± 0.2 | 51 ± 2 | 41 ± 2 | 1.2 ± 0.2 |

Table III: Elemental compositions of the direct CCP-PEALD ZnO films, measured using ToF-ERDA.

| P (W) | t (s) | H (at. -%) | C (at. -%) | N (at. -%) | O (at. -%) | Zn (at. -%) | O/Zn ratio |
|---|---|---|---|---|---|---|---|
| 50 | 3 | 10 ± 1 | 3 ± 0.5 | 0.8 ± 0.1 | 51 ± 2 | 35 ± 2 | 1.5 ± 0.2 |
| 50 | 6 | 8 ± 0.5 | 2 ± 0.2 | 0.5 ± 0.1 | 51 ± 2 | 38 ± 2 | 1.4 ± 0.2 |
| 100 | 3 | 8 ± 0.5 | 2.5 ± 0.2 | 1 ± 0.2 | 52 ± 2 | 36 ± 2 | 1.5 ± 0.2 |
| 100 | 6 | 5 ± 0.5 | 0.7 ± 0.1 | 0.4 ± 0.1 | 52 ± 2 | 42 ± 2 | 1.2 ± 0.2 |
| 200 | 3 | 6 ± 0.5 | 1.7 ± 0.2 | 0.9 ± 0.1 | 52 ± 2 | 39 ± 2 | 1.3 ± 0.2 |
| 200 | 6 | 5 ± 0.5 | 0.5 ± 0.1 | 0.5 ± 0.1 | 52 ± 2 | 42 ± 2 | 1.2 ± 0.2 |

List of figure captions:

Figure 1: The growth per cycle of the ZnO films deposited on Si substrate with (a) ICP-PEALD, (b) remote CCP-PEALD, and (c) direct CCP-PEALD. Empty symbols in (b) denote the films deposited with alternative $O_2$ feed distribution and plasma ignition with $N_2$. Error bars correspond to variation in the measured film thickness over the deposition area.

Figure 2: The Zn intake per cycle, measured with Rutherford backscattering spectrometry from ZnO films deposited on Si, PMMA, and PC substrates using (a) ICP-PEALD, (b) remote CCP-PEALD, and (c) direct CCP-PEALD. The empty symbols in (b) denote the films deposited with alternative gas feed and plasma ignition with $N_2$.

Figure 3: ATR-FTIR absorption spectra of the ZnO films on PC (solid lines) and PMMA (dashed lines). The substrate signal is subtracted from the spectra. ZnO deposited using (a) ICP-PEALD with 500 W plasma power and 6 s plasma pulses, (b) ICP-PEALD with 2000 W power and 6 s pulses, (c) remote CCP-PEALD with 50 W power and 3 s pulses, (d) remote CCP-PEALD with 50 W power and 3 s pulses using the alternative $O_2$ feed, and (e) direct CCP-PEALD with 50 W power and 3 s pulses.

Figure 4: XRD patterns of the ZnO films deposited with (a) ICP-PEALD, with 11 s plasma pulses, (b) remote CCP-PEALD and (c) direct CCP-

PEALD, both with 6 s plasma pulses.

Figure 5: Atomic force micrographs of the ICP-PEALD ZnO films deposited on Si substrate with plasma power of (a) 500 W, (b) 1000 W, and (c) 2000 W, all with 11 s plasma pulses. The corresponding RMS roughnesses are (a) 0.3 ± 0.1 nm, (b) 0.8 ± 0.1 nm, and (c) 1.2 ± 0.1 nm.

Figure 6: Atomic force micrographs of the remote CCP-PEALD ZnO films deposited on Si substrate with plasma power of (a) 50 W, (b) 100 W, and (c) 200 W, all with 6 s plasma pulses. The corresponding RMS roughnesses are (a) 2.2 ± 0.1 nm, (b) 2.9 ± 0.1 nm, and (c) 1.4 ± 0.1 nm.

Figure 7: Atomic force micrographs of the direct CCP-PEALD ZnO films deposited on Si substrates with plasma power of (a) 50 W, (b) 100 W, and (c) 200 W, all with 6 s plasma pulses. The corresponding RMS roughnesses are (a) 2.6 ± 0.1 nm, (b) 2.6 ± 0.1 nm, and (c) 2.20 ± 0.1 nm.

Figure 8: Atomic force micrographs of the PEALD ZnO films on the PMMA substrate, (a) uncoated PMMA reference, ZnO deposited with (b) ICP-PEALD, plasma power 1000 W, 11 s pulses, (c) remote CCP-PEALD, plasma power 100 W, 6 s pulses, and (d) direct CCP-PEALD, plasma power 100 W, 6 s pulses.

Figure 9: Atomic force micrographs of the PEALD ZnO films on the PC substrate, (a) uncoated PC reference, ZnO deposited with (b) ICP-PEALD, plasma power 1000 W, 11 s pulses, (c) remote CCP-PEALD, plasma power 100 W, 6 s pulses, and (d) direct CCP-PEALD, plasma power 100 W, 6 s pulses.

Figure 10: Atomic force micrographs of the PC surfaces after 15 min exposure to (a) UV/VUV irradiation of the $O_2$ plasma through the $MgF_2$ window, and (b) direct plasma. Both exposures were done using CCP-PEALD setup.

Figure 11: Optical emission spectra of the ICP-PEALD Ar–$O_2$ plasma with plasma powers of 500, 1000, and 2000 W. The spectra are normalized to the highest peak intensity of each spectrum. Inset: corresponding integration time -normalized spectra at wavelength range 650-860 nm.

Figure 12: Left: ICP plasma generator output frequency, DC Voltage, and DC current as a function of the applied power. Right: Ar 751 nm, Ar 811 nm, and O 777 nm peak intensities of the OES spectra as a function of applied power, normalized to the highest Ar intensity. The E–H transition region is highlighted with grey.

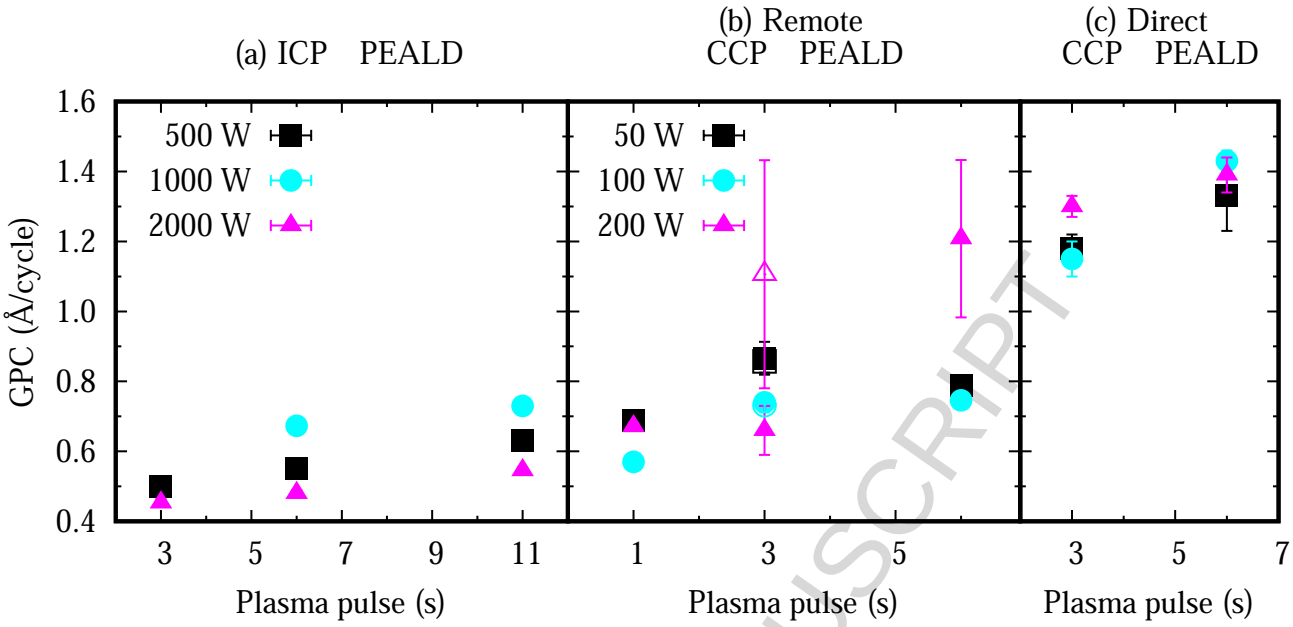


Figure 1:

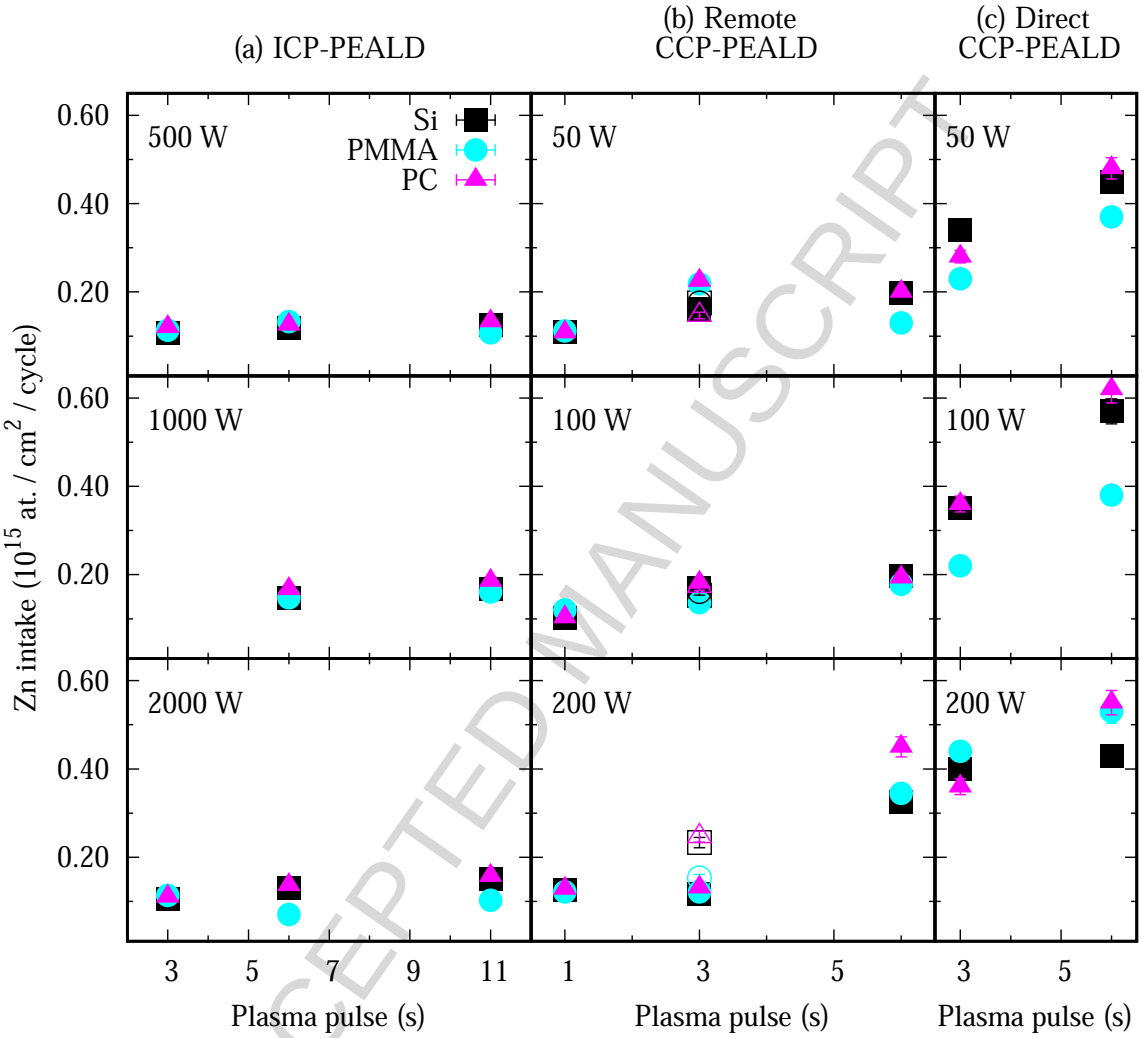


Figure 2:

Table IV: Representative examples of RMS roughness values of ZnO films on Si, PMMA, and PC substrates, and RMS roughnesses of PMMA and PC exposed to direct plasma and plasma UV through $MgF_2$ window.

| (a) ICP-PEALD | | | (b) Remote CCP-PEALD | | | (c) Direct CCP-PEALD | | |
|---|---|---|---|---|---|---|---|---|
| P (W) | t (S) | $R_{RMS}$ (nm) | P (W) | t (s) | $R_{RMS}$ (nm) | P (W) | t (s) | $R_{RMS}$ (nm) |
| Si (ref. 0.2 ± 0.02 nm) | | | | | | | | |
| 500 | 6 | 0.4 ± 0.1 | 50 | 3 | 1.8 ± 0.2 | 59 | 3 | 2.6 ± 0.1 |
| 500 | 11 | 0.3 ± 0.1 | 50 | 6 | 2.2 ± 0.1 | 50 | 6 | 2.6 ± 0.1 |
| 1000 | 6 | 0.5 ± 0.1 | 100 | 3 | 3.0 ± 0.3 | 100 | 3 | 2.1 ± 0.1 |
| 1000 | 11 | 0.8 ± 0.1 | 100 | 6 | 2.9 ± 0.1 | 100 | 6 | 2.6 ± 0.1 |
| 2000 | 6 | 1.1 ± 0.1 | 200 | 3 | 2.1 ± 0.2 | 200 | 3 | 2.5 ± 0.1 |
| 2000 | 11 | 1.2 ± 0.1 | 200 | 6 | 1.4 ± 0.1 | 200 | 6 | 2.2 ± 0.1 |
| PMMA (ref. 6 ± 1 nm) | | | | | | | | |
| 1000 | 6 | 1.5 ± 0.3 | 100 | 6 | 6.0 ± 0.4 | 100 | 6 | 10 ± 1 |
| 2000 | 6 | 3.0 ± 0.2 | 200 | 6 | 12 ± 5 | 200 | 6 | 9 ± 2 |
| PC (ref. 0.4 ± 0.1 nm) | | | | | | | | |
| 1000 | 6 | 1.4 ± 0.2 | 100 | 6 | 2.3 ± 0.3 | 100 | 6 | 1.7 ± 0.3 |
| 2000 | 6 | 1.2 ± 0.1 | 200 | 6 | 2.0 ± 0.2 | 200 | 6 | 3.0 ± 0.2 |

| Plasma exposure | Direct | $MgF_2$ window |
|---|---|---|
| PMMA | 35 ± 5 nm | 6 ± 1 nm |
| PC | 1.3 ± 0.2 nm | 0.4 ± 0.1 nm |

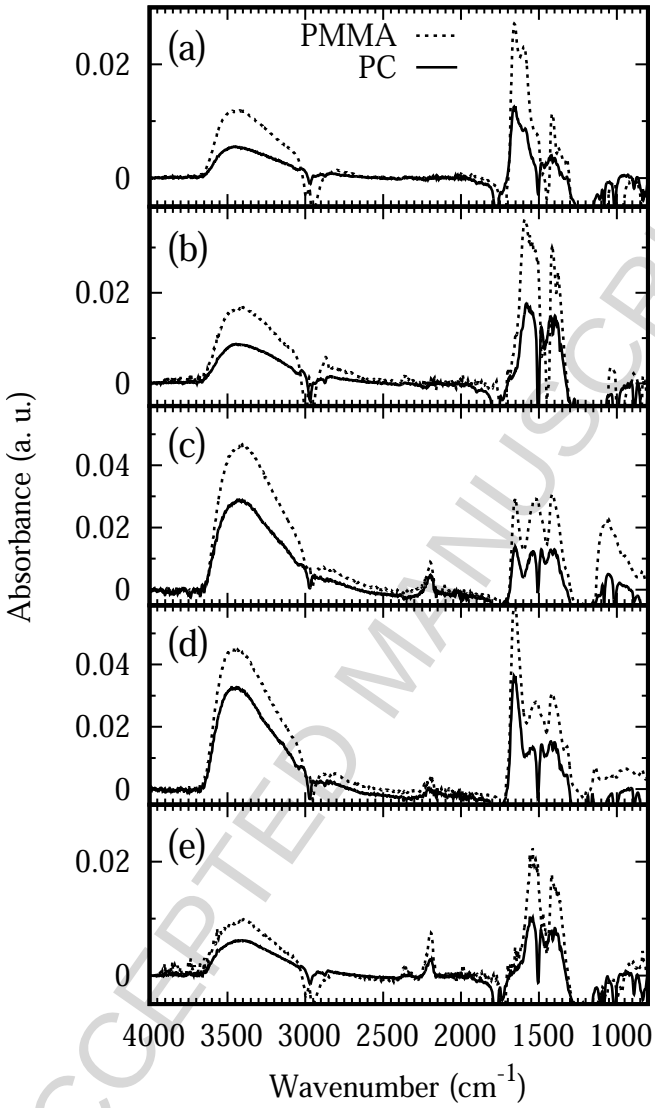


Figure 3:

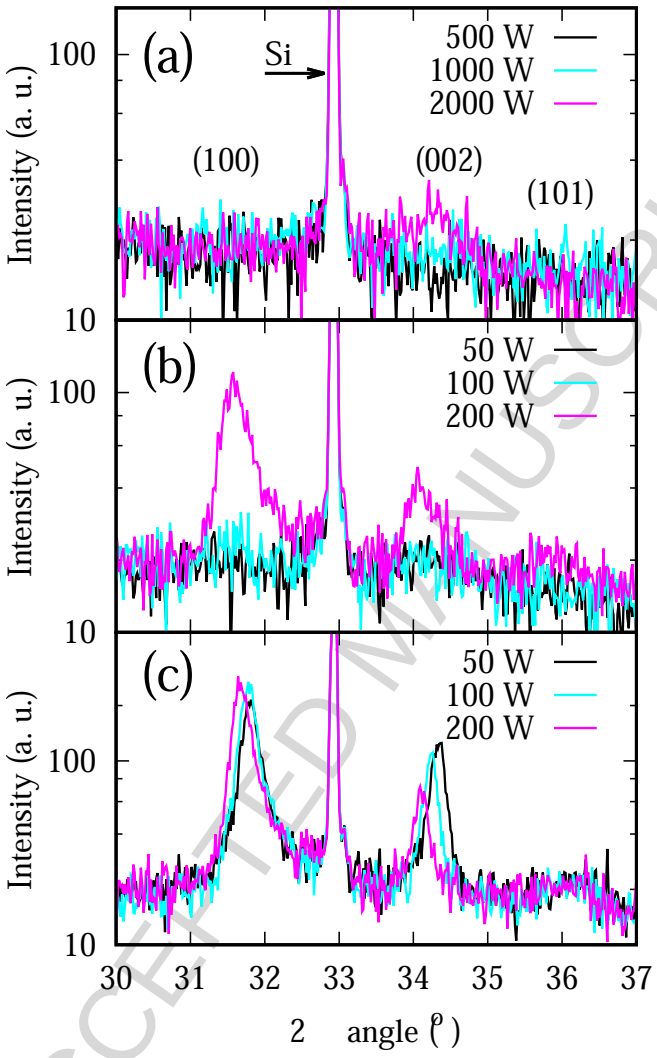


Figure 4:

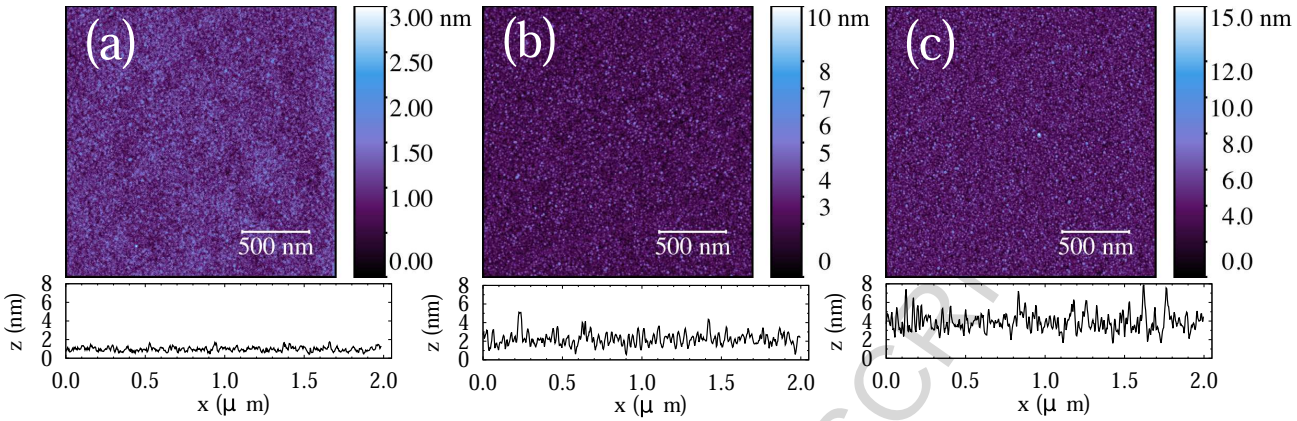


Figure 5:

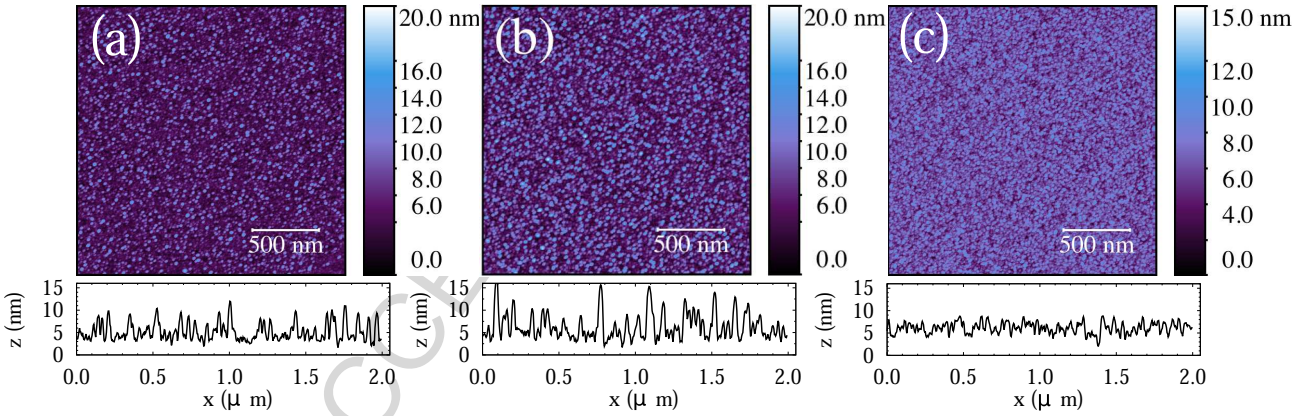


Figure 6:

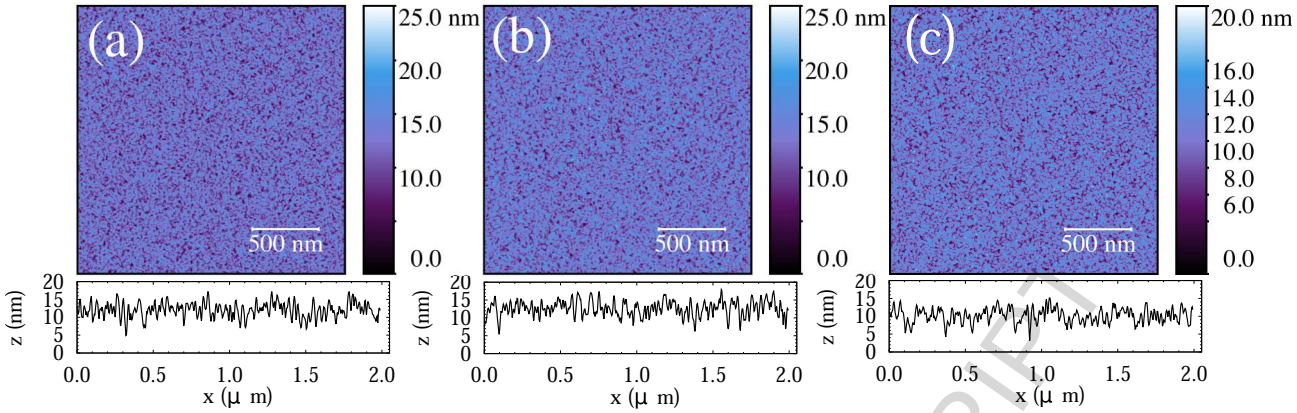


Figure 7:

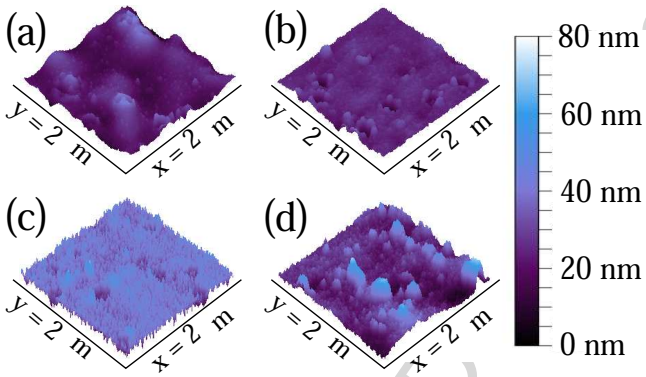


Figure 8:

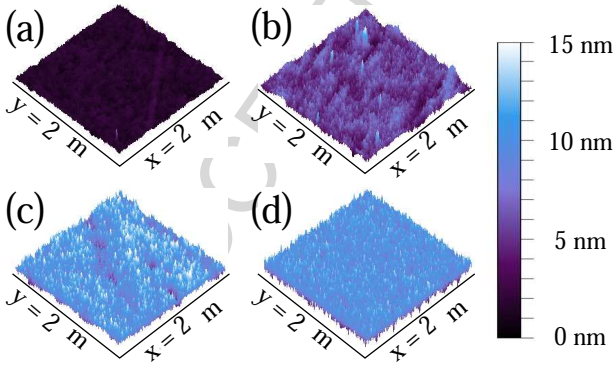


Figure 9:

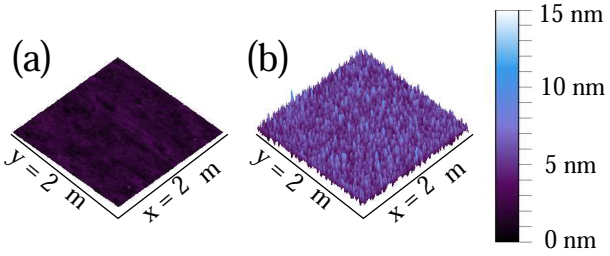


Figure 10:

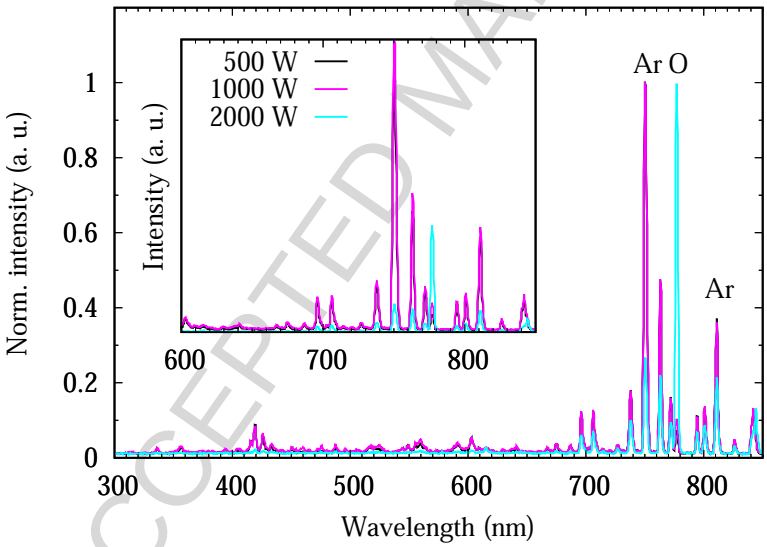


Figure 11:

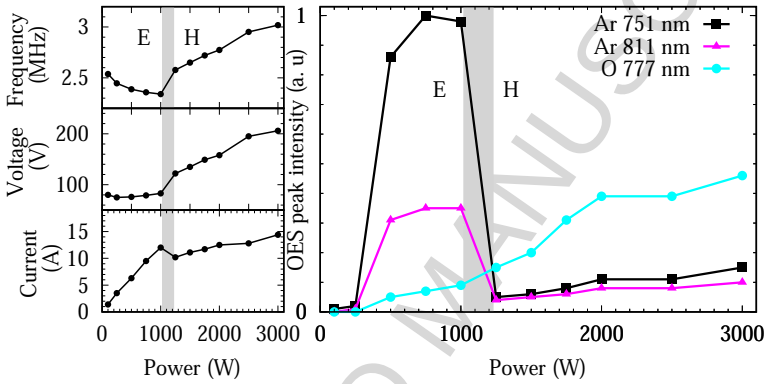


Figure 12:

**Highlights**

- ZnO films were grown using room-temperature PEALD with 3 different plasma configurations
- Film growth was similar on Si, PMMA, and PC substrates
- Use of remote PEALD results in amorphous ZnO with high O/Zn ratio
- Direct plasma produces polycrystalline ZnO films but damages the polymer substrates
- EH mode transition in the inductively coupled plasma was observed 49